Robust Vehicle Lateral Stabilization via Set-Based Methods for Uncertain Piecewise Affine Systems

G. Palmieri * **M. Barić** ** **F. Borrelli** ** **L. Glielmo** *

* *Department of Engineering, Universitá degli Studi del Sannio, Benevento, Italy; (e-mail: palmieri,glielmo@unisannio.it).*
** *Department of Mechanical Engineering, University of California, Berkeley, USA (e-mail: baric@berkeley.edu, fborrelli@me.berkeley.edu)*

Abstract: The paper presents the design of a lateral stability controller for ground vehicles based on front steering and four wheels independent braking. The control objective is to track yaw rate and lateral velocity reference signals while avoiding front and rear wheel traction force saturation. Control design is based on an approximate piecewise–affine nonlinear dynamical model of the vehicle. Vehicle longitudinal velocity and drivers steering input are modeled as measured disturbances taking values in a compact set. A time–optimal control strategy which ensures convergence into a maximal robust control invariant (RCI) set is proposed. This paper presents the uncertain model, the RCI computation, and the control algorithm. Simulations results on a high–fidelity vehicle model show the effectiveness of the propose scheme.

1. INTRODUCTION

The majority of commercial active safety systems are based on brake intervention. Antilock Braking Systems (ABS) (see Final Report of NHTSA [2000] for an introduction) and Electronic Stability Control (ESC) (van Zanten et al. [1995]) are two well known examples whose goals are to stabilize the longitudinal and yaw motion vehicle dynamics, respectively. Typically such systems are designed by combining local single–input single–output linear controllers and heuristic rules. Those controllers can be immediately implemented on low-cost hardware, but, on the other hand, they require extensive simulations and experimental testing to deliver high performances and robustness, which increases the cost of the overall design procedure.

In this work, we present a systematic approach to design yaw and lateral dynamics control. We model the nonlinear dynamics of vehicle as a PieceWise Affine (PWA) discrete–time system, whose states (yaw rate and lateral velocity) and control variables (front turn wheel angle and braking moment) are subject to hard constraints. Longitudinal velocity is treated as a state–dependent measured disturbance. This represents an improvement compared to the previous work of Palmieri et al. [2010], where the longitudinal speed is assumed to be constant over a given manoeuver.

We design a controller which guarantees constraints satisfaction at all times for all possible disturbance realizations using *set–theoretic methods* for control synthesis (Blanchini and Miani [2008]). In particular, we compute the robust control invariant (RCI) set for the piecewise–affine model of the vehicle using the results on *Max–min reachability* introduced in (Raković et al. [2008], Barić [2008]). Such RCI set constitutes the target set of a robust time–optimal control algorithm. To the best of our knowledge, this paper presents the first attempt to address hard constraints and uncertainties in the vehicle stability control system in a systematic and rigorous way through a robust constrained control design. The paper is structured as follows. In Section 2 we present the vehicle model. In Section 3, we present the controller design. Simulation results are reported in Section 4 followed by final remarks in Section 5.

Nomenclature and basic definitions We use standard notation for the set of natural numbers $\mathbb{N}$ and the set of real numbers $\mathbb{R}$. Given two sets $A \subseteq \mathbb{R}^n$ and $B \subseteq \mathbb{R}^n$, the complement of A is A^c and the set difference between A and B is $A \backslash B$. The *orthogonal projection* of a set $\mathcal{A} \subseteq \mathcal{X} \times \mathcal{Y} \subseteq \mathbb{R}^n \times \mathbb{R}^m$ onto $\mathcal{X}$ is defined as $\mathrm{Proj}_x(\mathcal{A}) := \{x \in \mathcal{X} \colon \exists y \in \mathcal{Y} \text{ such that } (x, y) \in \mathcal{A}\}$. A *polyhedron* is an intersection of a finite number of open and/or closed half-spaces. A *polytope* is a compact polyhedron. A union of finitely many (polytopes) polyhedra is referred to as a (compact) polygon. A set–valued mapping $\Gamma \colon \mathcal{X} \rightrightarrows \mathcal{Y}$ assigns to each element of $\mathcal{X}$ *a subset* (possibly empty set) of the set $\mathcal{Y}$. A graph of the set–valued mapping $\Gamma \colon \mathcal{X} \rightrightarrows \mathcal{Y}$, denoted as $\mathrm{gph}\Gamma$, is the set $\{(x, y) \colon x \in \mathcal{X} \text{ and } y \in \Gamma(x) \subseteq \mathcal{Y}\}$.

2. A MODEL OF THE LATERAL VEHICLE DYNAMICS

In this section, we describe the Hybrid PieceWise Affine (HPWA) bicycle model used for robust controller synthesis. We derive it starting from the standard nonlinear bicycle model [Rajamani, 2005, Sec. 2.3]. We use the following notation: the subscripts $(\cdot)_f$ and $(\cdot)_r$ denote variables associated with the front and rear wheel, respectively. Also, the subscript $()_\star$ stands for both $(\cdot)_f$ and $(\cdot)_r$.

The *bicycle model* (cf. Kienke [2000], Rajamani [2005], Falcone et al. [2008]) is given by

$$m\ddot{y} = -m\dot{x}\dot{\psi} + 2F_{c_f} + 2F_{c_r} \tag{1a}$$

$$I\ddot{\psi} = 2aF_{c_f} - 2bF_{c_r} + M \tag{1b}$$

where $\dot{y}$ is the lateral velocity, $\dot{x}$ is the longitudinal velocity, $\dot{\psi}$ is the yaw rate, M is the braking moment, $F_{c_\star}$ are the cornering tire forces, a is longitudinal distance from the vehicle's center of gravity (CoG) to the front axle, b is longitudinal distance from CoG to the rear axle and I is yaw inertia moment of vehicle around the z-axis. There exists a number of different models for cornering tire

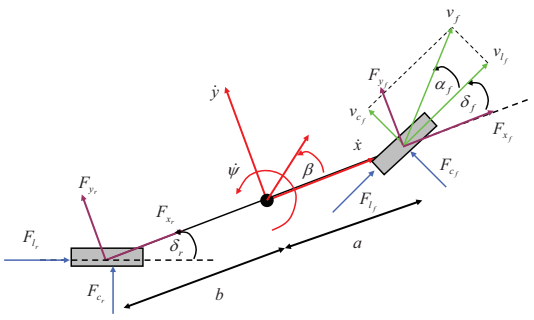

Fig. 1. The simplified "bicycle model" of the vehicle.

forces; in this work we are using the well-known *Pacejka's model* (Pacejka [2005]). In Pacejka's model the cornering forces are defined by a *static* non–linear mapping:

$$F_{c_\star} = f_c(\alpha_\star, s_\star, \mu_\star, F_{z_\star}), \tag{2}$$

with $s_\star$ slip ratios (the normalized difference between the longitudinal slip velocity and the forward speed of the wheel center, ([Pacejka, 2005, Sec. 2.2]), μ the friction coefficient, $\alpha_\star$ tire slip angles (the angle between the longitudinal axis of the tire frame and the tire velocity, see Figure 1) and $F_{z\star}$ normal tire forces. The mapping $f_c(\cdot)$ is given by the well-known *Pacejka's formulas* ([Pacejka, 2005, Sec. 4.3]). The dependence of the cornering (lateral) tire force on the slip angle α, for a fixed value of the slip ration $s = 0$, is depicted in Figure 2. Figure 2 also shows the PieceWise–Affine (PWA) approximation of the Pacejka's curve. This approximation is the starting point for derivation of the PWA dynamical model of the vehicle, discussed next.

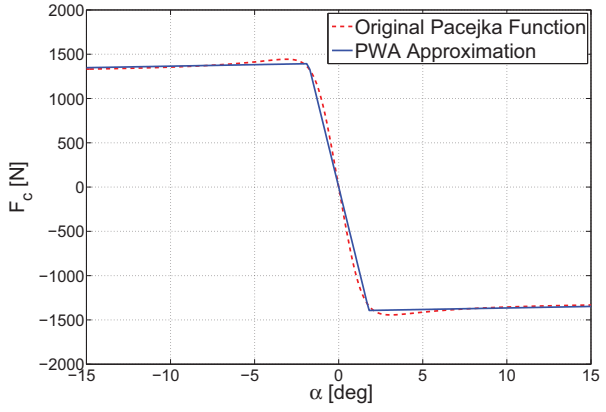

Fig. 2. Lateral tire force.

2.1 PWA Hybrid Model

In this section we use the approximation shown in Figure 2 of $f_c(\cdot)$. The following assumptions are used.

Assumption 1. The longitudinal velocity of the vehicle $\dot{x}$ is known and constant.

Assumption 2. The friction coefficient μ is known, constant and the same for both wheels of the bicycle model. Normal tire forces $F_{z\star}$ are assumed to be constant, known and the same for both wheels.

Under the above assumptions, it is reasonable to consider $F_{c\star}$ in their pure cornering condition ($s_\star = 0$) and depending only on the slip angles $\alpha_\star$. The dependence of forces $F_{c\star}$ on the states $\dot{y}$, $\dot{\psi}$ is derived as follows. Consider the slip angle definition:

$$\alpha_\star = \tan^{-1} v_{c,\star}/v_{l,\star}, \tag{3}$$

and assuming zero rear steering angle $\delta_r = 0$. We obtain the following relations

$$v_{l,f} = \dot{x} + \left(\dot{y} + a\dot{\psi}\right)\delta_f, \qquad v_{l,r} = \dot{x}, \tag{4a}$$

$$v_{c,f} = -\dot{x}\delta_f + \left(\dot{y} + a\dot{\psi}\right), \qquad v_{c,r} = \left(\dot{y} - b\dot{\psi}\right). \tag{4b}$$

Finally, substituting the equations (4) into the (3) and considering the "small angles assumption" (i.e. that $\tan^{-1}(x) \approx x$ for small x), we obtain the desired (approximate) dependence of the tire slip angels α_f and α_r:

$$\alpha_f = \frac{a\dot{\psi} + \dot{y}}{\dot{x}} - \delta_f, \quad \alpha_r = \frac{b\dot{\psi} - \dot{y}}{\dot{x}}. \tag{5}$$

The shape of the mapping $f_c(\cdot)$, as shown in Figure 2, is particulary amenable to piecewise–affine approximation. In its simplest form such approximation comprises three affine parts:

$$g_\star(\alpha_\star) = \begin{cases} c_s\alpha_\star + (c_l + c_s)\,\alpha_\star^\bullet, & \text{if } -\dfrac{\pi}{6} \le \alpha_\star \le -\alpha_\star^\bullet \\ -c_l\alpha_\star, & \text{if } -\alpha_\star^\bullet \le \alpha_\star \le \alpha_\star^\bullet \\ c_s\alpha_\star - (c_l + c_s)\,\alpha_\star^\bullet, & \text{if } \alpha_\star^\bullet \le \alpha_\star \le \dfrac{\pi}{6} \end{cases} \tag{6}$$

where the interval $[-\alpha_\star^\bullet, \alpha_\star^\bullet]$ represents the linear zone, the interval $[-\pi/6, -\alpha_\star^\bullet]$ marks the negative saturation zone and the positive interval $[\alpha_\star^\bullet, \pi/6]$ marks the positive saturation zone. We can now write the hybrid (PWA) bicycle model of the vehicle (Conte [2009]):

$$\begin{bmatrix}\ddot{y}\\ \ddot{\psi}\end{bmatrix} = \begin{bmatrix} -\dfrac{a_{11}(\alpha_f,\alpha_r)}{v_x} & -\dfrac{a_{12}(\alpha_f,\alpha_r)}{v_x} - v_x \\ -\dfrac{a_{21}(\alpha_f,\alpha_r)}{v_x} & -\dfrac{a_{21}(\alpha_f,\alpha_r)}{v_x} \end{bmatrix}_i \begin{bmatrix}\dot{y}\\ \dot{\psi}\end{bmatrix} + \begin{bmatrix} -b_{11}(\alpha_f,\alpha_r) & 0 \\ -b_{21}(\alpha_f,\alpha_r) & a_{22}(\alpha_f,\alpha_r)\end{bmatrix}_i \begin{bmatrix}\delta_f\\ M\end{bmatrix} + \begin{bmatrix}f_1\\ f_2\end{bmatrix}_i \tag{7}$$

where $v_x = \dot{x}$ and the coefficient a_{ij}, b_{ij}, f_i depend on vehicle parameters and on current value of α_f and α_r as described in (6).

In this work we substitute the Assumption 1 on the constant longitudinal velocity with the following one:

Assumption 3. The longitudinal velocity of the vehicle $\dot{x}$ is bounded within the interval $[v_{x_{(\min)}}, v_{x_{(\min)}}]$ and is known at each discrete–time instance.

Note that in our model the information is still limited as we do not take into account the dynamical evolution of the

longitudinal velocity, but rather treat it as a parametric variable whose dynamics is not known, but whose bounds are known and whose value can be obtained at each time instant. Also, under the new assumption the dependence of forces $F_{c\star}$ on the states $\dot{y}$, $\dot{\psi}$ in (2) is imprecise when a longitudinal slip is not equal to zero. This can be easily handled by using an additive input uncertainty as presented in Palmieri et al. [2010].

In the reminder of this section we will show how to rewrite model (7) into a form which is piecewise affine with bounded polyhedral parametric uncertainties. First of all we rewrite the model (7) as follows:

$$\dot{\xi} = \begin{bmatrix} a_{11} & a_{12} \\ a_{21} & a_{22} \end{bmatrix}_i \frac{\xi}{v_x} + \begin{bmatrix} 0 & -v_x^2 \\ 0 & 0 \end{bmatrix}_i \frac{\xi}{v_x} + B_i u + f_i. \tag{8}$$

where $\xi = [\dot{y}, \dot{\psi}]^T$ and $u = [\delta_f, M]^T$. We define:

$$\begin{aligned} \bar{A} &:= \begin{bmatrix} a_{11} & a_{12} \\ a_{21} & a_{22} \end{bmatrix}_i, & z &:= \frac{\xi}{v_x} \\ w_1 &:= -v_x^2 z(2), & \bar{B} &:= B_i, \\ \bar{f} &:= f_i \end{aligned} \tag{9}$$

and obtain the compact representation:

$$\dot{\xi} = \bar{A}_i z + \begin{bmatrix} 1 \\ 0 \end{bmatrix}_i w_1 + \bar{B}_i u + \bar{f}_i. \tag{10}$$

Using Euler's method and, with some abuse of notation, we can discretize the model (8):

$$\begin{aligned} \frac{\xi(k+1) - \xi(k)}{T_s} \approx & \bar{A}_i z(k) + \begin{bmatrix} 1 \\ 0 \end{bmatrix}_i w_1(k) + \bar{B}_i u(k) + \bar{f}_i \\ \xi(k+1) = & \hat{A}_i z(k) + \hat{B}_i u(k) + \hat{f}_i + w_z(k) \end{aligned} \tag{11}$$

thus obtaining

$$\begin{aligned} \hat{A} &:= T_s \bar{A}, & \hat{B} &:= T_s \bar{B} \\ \hat{f} &:= T_s \bar{f}, & w_z(k) &:= T_s \begin{bmatrix} 1 \\ 0 \end{bmatrix}_i w_1(k) + \xi(k). \end{aligned}$$

In model (11) the evolution of the state vector ξ is defined by the linear expression in $z = \xi / v_x$, whose value is precisely known at each time instance.

Using the definition of z in (9), we can rewrite the equation (5) as follows:

$$\alpha_f = a z_1 + z_2 - \delta_f, \quad \alpha_r = b z_1 - z_2. \tag{12}$$

The constraints on z as defined by (6) and (12) are linear. Next we define the bounds for the disturbance vector w_z in (11).

Recall that the components of the vector w_z are:

$$w_{z_1} := v_x z_1 - T_s v_x^2 z_2, \tag{13a}$$
$$w_{z_2} := v_x z_2, \tag{13b}$$

w_z is a nonlinear functions of z and v_x and unsuitable for the robust control design based on polyhedral uncertainties. For this reason we over–approximate the bounds on the components of the vector w_z by a union of polytopes. For the first component (w_{z_1}), the signs of z_1 and z_2 define four cases, S1 to S4, as indicated in Table 2.1. The bounds on w_{z_1} for each of these cases are then obtained by fixing the extreme value of longitudinal velocity ($v_{x_{\min}}$ and $v_{x_{\max}}$). The approximation for the case when both z_1 and z_2 are positive is given in Figure 3. The union $W_{z_1} = \bigcup_{i=1}^{4} W_{z_1}^i$ represents the conservative polyhedral

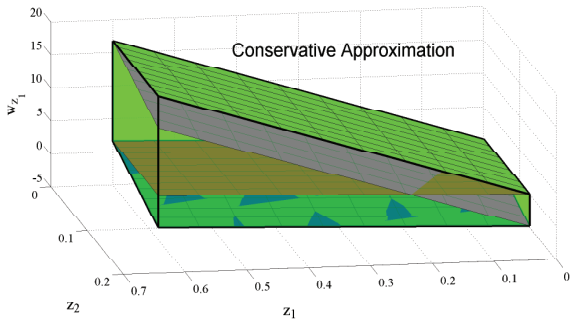

Fig. 3. The polytope over–approximating the domain of the disturbance w_{z_1} for Scenario 1 (see Table 2.1).

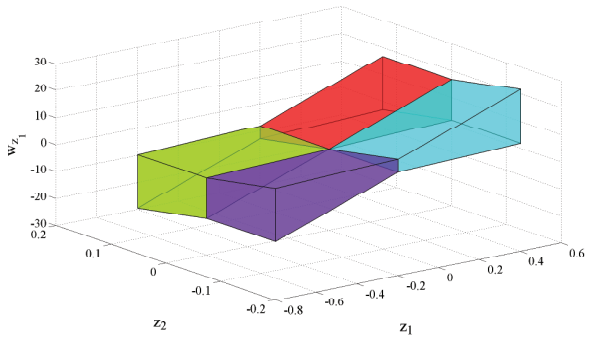

Fig. 4. Polyhedral approximation of the bounds on the disturbance w_{z_1}.

Table 1. Computation of w_{z_1} hard constraints

S 1	$z_1 \geq 0$	$z_2 \geq 0$	$w_{z_1} = v_{x_{\min}} z_1 - T_s v_{x_{\min}}^2 z_2$
			$w_{z_1} = v_{x_{\min}} z_1 - T_s v_{x_{\max}}^2 z_2$
			$w_{z_1} = v_{x_{\max}} z_1 - T_s v_{x_{\min}}^2 z_2$
			$w_{z_1} = v_{x_{\max}} z_1 - T_s v_{x_{\max}}^2 z_2$
S 2	$z_1 \leq 0$	$z_2 \geq 0$	$w_{z_1} = v_{x_{\min}} z_1 - T_s v_{x_{\min}}^2 z_2$
			$w_{z_1} = v_{x_{\min}} z_1 - T_s v_{x_{\max}}^2 z_2$
			$w_{z_1} = v_{x_{\max}} z_1 - T_s v_{x_{\min}}^2 z_2$
			$w_{z_1} = v_{x_{\max}} z_1 - T_s v_{x_{\max}}^2 z_2$
S 3	$z_1 \geq 0$	$z_2 \leq 0$	$w_{z_1} = v_{x_{\min}} z_1 - T_s v_{x_{\min}}^2 z_2$
			$w_{z_1} = v_{x_{\min}} z_1 - T_s v_{x_{\max}}^2 z_2$
			$w_{z_1} = v_{x_{\max}} z_1 - T_s v_{x_{\min}}^2 z_2$
			$w_{z_1} = v_{x_{\max}} z_1 - T_s v_{x_{\max}}^2 z_2$
S 4	$z_1 \leq 0$	$z_2 \leq 0$	$w_{z_1} = v_{x_{\min}} z_1 - T_s v_{x_{\min}}^2 z_2$
			$w_{z_1} = v_{x_{\min}} z_1 - T_s v_{x_{\max}}^2 z_2$
			$w_{z_1} = v_{x_{\max}} z_1 - T_s v_{x_{\min}}^2 z_2$
			$w_{z_1} = v_{x_{\max}} z_1 - T_s v_{x_{\max}}^2 z_2$

approximation for the state–dependent bounds of the disturbance component w_{z_1} and we report it in Figure 4. The second component of the disturbance (w_{z_2}) satisfies the following linear inequalities:

$$z_{2_{\min}} \leq z_2 \leq z_{2_{\max}} \tag{14a}$$
$$v_{x_{\max}} z_2 - w_{z_2} \leq 0 \tag{14b}$$

which define the set W_{z_2}. Note that the equations (6), (11) and (12) provide a hybrid dynamical system with nine distinct dynamic behaviors described by linear (affine) difference equations. The actual dynamic behavior of the system is determined by the value of the side slip angles α^* according to (6). Using the relations (12) the hybrid bicycle model (11) can be compactly written:

$$\xi^+ = \hat{A}_i z + \hat{B}_i u + \hat{f}_i + w_z, \quad \text{if } (z,u) \in \mathcal{Q}_i, i \in \{1,2,\ldots,9\}, \quad w_z \in \mathcal{W}(z) \tag{15}$$

where $z = [\frac{\dot{y}}{v_x}; \frac{\dot{\psi}}{v_x}]^T$, $\{\mathcal{Q}_i\}_{i=1}^9$ is a collection of *polyhedral regions* in $\mathbb{R}^4$ defining the regions for each dynamic behavior and *constraints on the scaled state and control variables* and $\mathcal{W}(\cdot)$ is the graph of mapping and it is defined by (14) and polygonal approximation of bounds on w_{z_1} .

3. ROBUST CONTROL DESIGN

In this section we describe the robust control strategy for our Robust Electronic Stability Controller (RESC). The primary task of RESC is to maintain the "nominal" behavior of the vehicle such that neither front nor rear tire forces are saturated *for any possible values of the longitudinal velocity*. We formalize these notions by set–theoretic terms – in particular robust control invariance and constrained controllability for the considered system class affected by state–dependent uncertainties. In our case the realization of uncertainties is available (known via measurement) to the controller at each discrete–time instance. Such type of robust control is typically known as *full-information feedback* control. We will refer to it as "max–min" robust control (Barić et al. [2008]). In this section we provide only the details relevant to our problem. For supplementary discussion on the topic the reader is referred to Raković et al. [2008], Barić [2008].

3.1 Approximate Max–min Reachability for the Bicycle PWA Model

Our goal is to synthesize the constrained controller for the system (8) in discrete–time which will ensure robust constraint satisfaction for the anticipated variations of longitudinal velocity v_x. Consider the discrete–time version of the model (8):

$$\xi^+ = f_d(\xi, u, v_x). \tag{16}$$

The variables (ξ, u, v_x) are subject to constraints:

$$v_x \in \mathcal{V}_x, \quad (\xi, u) \in \mathcal{C}_{\xi u}, \tag{17}$$

where $\mathcal{V}_x := \left[v_x^{\min}, v_x^{\max}\right]$ and $\mathcal{C}_{\xi u} \subset \mathbb{R}^n \times \mathbb{R}^m$ is the set of joint constraints on the state ξ and the control input u. As stated in Assumption 3, the value of v_x is known (exactly measured) in each time instance. Theoretical framework for robust control of constrained discrete–time systems subject to measured perturbations (disturbances) is given in Raković et al. [2008], Barić [2008] under the name *max–min reachability*. The fundamental notion in this framework, and any other discrete–time constrained robust control problem, is the notion of *controllable* or *backwards–reachable sets*. Given the target sets $\mathcal{X}$, the backwards–reachable set is the set of initial state vectors from which the target set $\mathcal{X}$ can be reached by an admissible control action. More precisely, in our *max–min* setup and for the dynamical system (16) and the constraints (17), the one–step backwards–reachable set is given by the following mapping:

$$Pre(\mathcal{X}) := \{\xi \colon \forall v_x \in \mathcal{V}_x \; \exists u \text{ such that } (\xi, u) \in \mathcal{C}_{\xi u} \text{ and } f_d(\xi, u, v_x) \in \mathcal{X}\}. \tag{18}$$

The computation of the $Pre(\mathcal{X})$ for a given target set $\mathcal{X}$ is essential for the robust control sysnthesis for our problem. However, as already hinted, the model based on (8) and (16) is not suitable for the available efficient computational methods which are mostly based on operations on polyhedral sets (like Multi–Parametric Toolbox (Kvasnica et al. [2003]) used in this paper). For this reason, instead of using the the model (8) and (16)–(17), we introduce a conservative approximation given by (15). We can write the model (15) compactly as:

$$\xi^+ = f_{pwa}(z, u, w_z), \quad \text{subj. to } (z,u) \in \mathcal{C}_{zu},\ w_z \in \mathcal{W}(z),$$

where the constraint set $\mathcal{C}_{zu}$ is given as a union of polyhedra $\mathcal{Q}_i$ in (15) and the graph of mapping $\mathcal{W}(\cdot)$ is defined by inequalities (14) and the polygonal approximation of bounds on w_{z1} discussed in Section 2.1 and shown in Figure 4. Given the target set $\mathcal{X}$, the *max–min* controllable set $Pre_\xi(\mathcal{X})$ for the dynamical system (19) is defined by the following expressions:

$$Pre_z(\mathcal{X}) := \{z \colon \forall w_z \in \mathcal{W}(z) \; \exists u \text{ such that } (z,u) \in \mathcal{C}_{zu} \text{ and } f_{pwa}(z,u,w_z) \in \mathcal{X}\}, \tag{20a}$$

$$Pre_\xi(\mathcal{X}) := \left\{\xi \colon \frac{\xi}{v_x} \in Pre_z(\mathcal{X}),\ \forall v_x \in \mathcal{V}_x\right\}. \tag{20b}$$

The computation of $Pre_z(\mathcal{X})$ in (20a) is performed by the algorithm introduced in (Raković et al. [2008], Barić [2008]) and reported here for completness.

Define the global constraints on (x, u, w_z) as

$$\Omega := \mathcal{C}_{zu} \times \text{gph}\mathcal{W}, \tag{21}$$

and its projections:

$$\Omega_{zw} := \text{Proj}_{zw_z}(\Omega), \quad \Omega_z := \text{Proj}_z(\Omega).$$

For a given target set $\mathcal{X} \subset \mathbb{R}^n$ define:

$$\Phi(\mathcal{X}) := \{(z,u,w_z) \in \Omega \colon \; f_{pwa}(z,u,w_z) \in \mathcal{X}\}, \tag{22a}$$

$$\Psi(\mathcal{X}) := \text{Proj}_{\Omega_{zw_z}}(\Phi(\mathcal{X})), \tag{22b}$$

$$\Delta(\mathcal{X}) := \Omega_{zw_z} \backslash \Psi(\mathcal{X}). \tag{22c}$$

Theorem 3.1. (Raković et al. [2008], Barić [2008]). For a given target set $\mathcal{X}$ the set $Pre_z(\mathcal{X})$ defined by (20a) can be computed as:

$$Pre_z(\mathcal{X}) = \Omega_z \backslash \text{Proj}_z(\Delta(\mathcal{X})), \tag{23}$$

where $\Delta(\mathcal{X})$ is given by (22c).

It remains to specify how to compute the set $Pre_\xi(\mathcal{X})$ defined by (20b). In our particular case, all considered sets (the constraints $\mathcal{C}_{\xi u}, \mathcal{C}_{zu}$ and the target set $\mathcal{X}$) are compact polygonal sets, i.e. given by a union of finitely many polytopes. From the discussion in Section 2.1 it can be seen that the mappings $f_{pwa}(\cdot)$ and $\mathcal{W}(\cdot)$ are continuous. Consequently, as established in Barić [2008], for a compact target set $\mathcal{X}$, the set $Pre_z(\mathcal{X})$ is also compact (possibly empty). If $\mathcal{X}$ is a compact polygonal set, the resulting $Pre_z(\mathcal{X})$, if not empty, can be represented as:

$$Pre_z(\mathcal{X}) = \bigcup_{i=1}^{q} \mathcal{P}_i, \tag{24}$$

for some $q \in \mathbb{N}$, where $\mathcal{P}_i$ are polytopes:

$$\mathcal{P}_i = \left\{z \colon H^i z \le k^i\right\},\ i \in \{1,\ldots,q\}.$$

Therefore, the set $Pre_\xi(\mathcal{X})$ for $Pre_z(\mathcal{X})$ given by (24) can be written as:

$$Pre_\xi(\mathcal{X}) = \left\{\xi \colon \frac{\xi}{v_x} \in \bigcup_{i=1}^{q} \mathcal{P}^i,\ \forall v_x \in \mathcal{V}_x\right\}.$$

Consider the sets:

$$\mathcal{P}_i^{\xi v_x} := \left\{(\xi, v_x)\colon H^i\xi - k^i v_x \le 0\right\}.$$

Clearly, $\xi/v_x \in \mathcal{P}_i$ if and only if $(\xi, v_x) \in \mathcal{P}_i^{\xi v_x}$. The set $Pre_\xi(\mathcal{X})$ can then be computed as:

$$Pre_\xi(\mathcal{X}) = \Omega_\xi \backslash \mathrm{Proj}_\xi\left(\left\{\Omega_{\xi v_x} \setminus \bigcup_{i=1}^{q} \mathcal{P}_i^{\xi v_x}\right\}\right), \qquad (25)$$

where:

$$\Omega_\xi := \mathrm{Proj}_\xi\left(\mathcal{C}_{\xi u}\right), \quad \Omega_{\xi v_x} := \Omega_\xi \times \mathcal{V}_x,$$

and the sets $\mathcal{C}_{\xi u}$ and $\mathcal{V}_x$ are the constraint sets as specified in (17). To see that (25) holds true, note that the second term in (25) (the projection $\mathrm{Proj}_\xi(\cdot)$) represents the set of all states ξ such that for some $v_x \in \mathcal{V}_x$ the ratio ξ/v_x is not in $Pre_z(\mathcal{X})$. The complement of that set with respect to Ω_ξ is, therefore, the set of states for which $\xi/v_x \in Pre_z(\mathcal{X})$ for all $v_x \in \mathcal{V}_x$. Note also that in case when $Pre_z(\mathcal{X}$ is a single polytope, i.e. $Pre_z = \{z\colon Hz \le k\}$, the set $Pre_\xi(\mathcal{X})$ is simply given as:

$$Pre_\xi(\mathcal{X}) = \{H\xi \le k v_x^{\min}\} \cap \{H\xi \le k v_x^{\max}\}. \qquad (26)$$

Operations on sets required to perform computations in (22)–(23) and (25) for polygonal constraints and target set $\mathcal{X}$ are available as part of several computational geometry toolboxes, MPT Toolbox (cf. Kvasnica et al. [2003]) being one of them. Therefore the mapping $Pre_\xi(\cdot)$ for the case of polygonal argument sets and constraints can be readily implemented and used for the computation of the robust *max–min* controller, as we discuss next.

3.2 Max–min robust control strategy for ESC

The primary task of Robust ESC (RESC) controller is to preserve "nominal" behavior of the car for all possible values w_z considered in the design. The "nominal" behavior is defined by the inequalities $|\alpha_\star| \le \alpha_\star^*$ in equation (6) and corresponds to the linear regime of both the front and the rear tire. In our PWA model (15), the vehicle is in the linear mode at time k if $(z_k, u_k) \in \mathcal{Q}_1$. For this reason we will refer to the linear regime of the tires as "mode 1". In our discrete–time setting, the desired control action u_k at any time instant k must satisfy $(z_k, u_k) \in \mathcal{Q}_1$ and at the same time $\xi_{k+1}/v_x(k+1) \in \mathrm{Proj}_z\left(\mathcal{Q}_1\right)$ *for all possible* $v_x(k+1)$, i.e. for all $v_x(k+1) \in \mathcal{V}_x$. Let

$$\mathrm{Proj}_z\left(\mathcal{Q}_i\right) = \left\{z\colon H^1 z \le k^1\right\},$$

and define $\mathcal{P}_1$ as follows:

$$\mathcal{P}_1 = \{\xi\colon H^1\xi \le k^1 v_x^{\min}\} \cap \{\xi\colon H^1\xi \le k^1 v_x^{\max}\}. \qquad (27)$$

We formalize the notion of robustness to velocity variations by defining *mode 1 robust control invariant (RCI)* set:

Definition 1. A set $\mathcal{R} \subseteq \mathcal{P}_1$ is called *mode 1 RCI set* for the dynamical system (15) if for every $\xi \in \mathcal{R}$ and each $(v_x, w_z) \in \mathcal{V}_x \times \mathcal{W}(\xi/v_x)$ there exists a control u such that $(\xi/v_x, u) \in \mathcal{Q}_1$ and $\hat{A}_1\xi/v_x + \hat{B}_1 u + \hat{f}_1 + w_z \in \mathcal{R}$.

For our purposes it is desirable to characterize the maximal mode 1 RCI set $\mathcal{R}_\infty^1$ which contains all other mode 1 RCI sets and it can be obtain using the standard iterative procedure (cf. Bertsekas [1972]), given by Algorithm 3.2.

In Algorithm 1 we perform computations of backwards–reachable sets only for the constraints and the dynamics

Algorithm 1 Computation of the set $\mathcal{R}_\infty^1$

$i = 0$;
$\mathcal{X}_i = \mathcal{P}_1$;
repeat
  i=i+1;
  $\mathcal{X}_i = Pre_\xi^1(\mathcal{X}_{i-1}) \cap \mathcal{X}_{i-1}$;
until $\mathcal{X}_i == \mathcal{X}_{i-1}$;
$\mathcal{R}_\infty^1 = \mathcal{X}_i$;

associated to the mode 1. In particular, the mapping $Pre_\xi^1(\cdot)$ used in Algorithm 1 is given by:

$$Pre_z^1(\mathcal{X}) := \{z\colon \forall w_z \in \mathcal{W}(z)\ \exists u \text{ such that } (z,u) \in \mathcal{Q}_1 \text{ and } \hat{A}_1 z + \hat{B}_1 u + \hat{f}_1 + w_z \in \mathcal{X}\},$$

$$Pre_\xi^1(\mathcal{X}) := \left\{\xi\colon \frac{\xi}{v_x} \in Pre_z^1(\mathcal{X}),\ \forall v_x \in \mathcal{V}_x\right\}.$$

If the Algorithm 1 terminates in finitely many iterations i_t, the set $\mathcal{R}_\infty^1 = \mathcal{X}_{i_t}$. The set $\mathcal{R}_\infty^1$ can be empty, or for a general dynamical system the Algorithm 1 may not converge in finitely many iterations. Figure 5 shows the outcome of the Algorithm 1 for our model with tire–road friction coefficient $\mu = 0.3$ and the longitudinal velocity range $\mathcal{V}_x = [40, 50]$ [km/h]. To the set $\mathcal{R}_\infty^1$ we associate

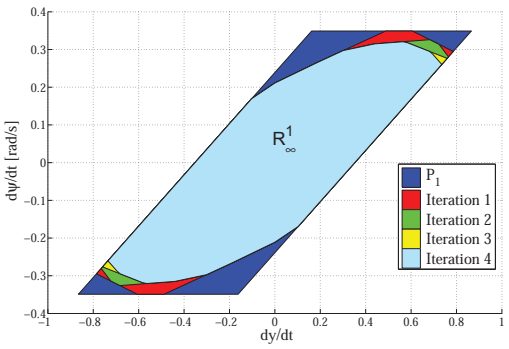

Fig. 5. Maximal mode 1 RCI set $\mathcal{R}_\infty^1$ for $\mu = 0.3$ and $40 \le v_x \le 50$ [kmh] and the outputs of Agorithm 1 intermediate iterations.

the control mapping $\mathcal{U}_\infty^1(\cdot)$ non–empty for all $\xi \in \mathcal{R}_\infty^1$ and all $v_x \in \mathcal{V}_x$:

$$\mathcal{U}_\infty^1(z, w_z) = \{u\colon (z,u) \in \mathcal{Q}_1, w_z \in \mathcal{W}(z) \text{ and } \hat{A}_1 z + \hat{B}_1 u + \hat{f}_1 + w_z \in \mathcal{R}_\infty^1\}. \qquad (28)$$

For a given scaled state vector z, any control input selected from the set $\mathcal{U}_\infty^1(z)$ results in the successor state ξ^+ being inside the set $\mathcal{R}_\infty^1$.

The maximal mode 1 RCI set is computed under certain assumption on uncertainties described by the vector w_z and advanced ESP controller can keep the state trajectory within the set $\mathcal{R}_\infty^1$ using braking and steering wheel angle for all admissible values of w_z. However, additional uncertainties that are not taken into account during the controller computation may drive the state vector outside the set $\mathcal{R}_\infty^1$. This can be due, for instance, to short–term variations of the friction coefficient or a sudden gust of wind. Also, the RESC may be activated by the driver at the moment when the state $\xi \notin \mathcal{R}_\infty^1$, e.g. when the vehicle is over-steering or under-steering. In such situations the

RESC scheme should bring the state back to the set $\mathcal{R}^1_\infty$. For that purpose we compute the k–step controllable sets $\mathcal{X}_k$:

$$\mathcal{X}_k = Pre_\xi(\mathcal{X}_{k-1}),\ k \geq 1, \tag{29}$$

with $\mathcal{X}_0 = \mathcal{R}^1_\infty$. To each controllable set $\mathcal{X}_k$, $k \geq 1$, we associate the control mapping:

$$\begin{aligned}\mathcal{U}_k(z, w_z) \ = \{u\colon (z,u) \in \mathcal{C}_{zu}, w_z \in \mathcal{W}(z) \text{ and} \\ f_{pwa}(z,u,w_z) \in \mathcal{X}_{k-1}\}\,.\end{aligned} \tag{30}$$

The value of the mapping $\mathcal{U}_k(\cdot)$ is non–empty for all $\xi \in \mathcal{X}_k$ and for all $v_x \in \mathcal{V}_x$. Figure 6 depicts the k–step controllable sets $\mathcal{X}_k$ for $\mu = 0.3$ and $40 \leq v_x \leq 50$ [km/h]. All the computations briefly outlined above are

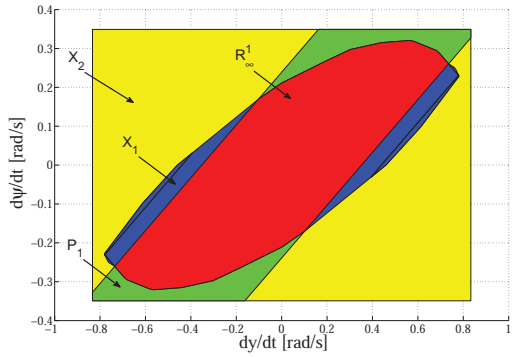

Fig. 6. The 2–step controllable sets $\mathcal{X}_k$ for $mu = 0.3$ and $40 \leq v_x \leq 50$ [kmh]..

performed using Multi–Parametric Toolbox for Matlab Kvasnica et al. [2003].

3.3 Notes on implementation

The control scheme used in this paper is a modification of the classical ESC scheme van Zanten et al. [1995] and it is depicted in Figure 7. The "Vehicle", through its sensors and some "Observers" transmits the information on its dynamics to "Reference Generator" that computes state reference signals which the "RESC" needs to track by generating appropriate steering and braking values, while keeping the state in the set $\mathcal{R}^1_\infty$ or driving it into $\mathcal{R}^1_\infty$. In the actual implementation for simulation, the control

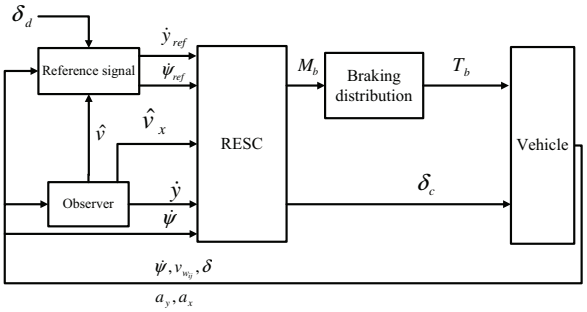

Fig. 7. General control scheme of electronic stability controller.

input u^* of the "RESC" is computed as:

$$\begin{aligned}u^* = &\arg \min_{u \in \mathcal{U}^1_\infty(z,w_z)} (\xi^+ - r)^T Q(\xi^+ - r) + \\ &+ (u - u_{\text{pre}})^T R(u - u_{\text{pre}}) + \rho(\delta_d - \delta_c),\end{aligned} \tag{31}$$

if $\xi \in \mathcal{R}^1_\infty$, or as:

$$u^* = \arg \min_{u \in \mathcal{U}_k(z,w_z)} (\xi^+ - r)^T Q(\xi^+ - r) + u^T R u, \tag{32}$$

for $\xi \in \mathcal{X}_i$ for $i \in \{1, 2\}$, where Q and R are suitably chosen matrices, ρ is a scalar that penalizes the difference between the turn wheel angle driver command and the control turn wheel angle, and $\mathcal{U}^1_\infty(\cdot)$ and $\mathcal{U}_k(\cdot)$ are control mappings defined by (28) and (30), respectively. As the PWA state–update mapping as well as the set–valued mapping $\mathcal{W}(z)$ in (15) are continuous and all constraint sets are compact, the mappings $\mathcal{U}^1_\infty(\cdot)$ and $\mathcal{U}_k(\cdot)$ are compact–valued (possibly empty), implying that the optimizer u^* in (31) and (32) is actually in the set of feasible solutions (if that one is non–empty).

Currently, all computations are formulated and performed with the aid of the YALMIP Toolbox Löfberg [2004]. For a real–time implementation one can use the Multi–Parametric Toolbox to obtain the explicit solution using parametric programming, in which case the robust control evaluation would reduce to a search in a look-up table of pre–computed optimal control inputs. For details the reader is referred to the instructive manual of the Multi–parametric Toolbox Kvasnica et al. [2003] and references therein.

4. SIMULATION RESULTS

In this section we validate the proposed control strategy in three simulation experiments. In the first one, we show that our control strategy is robust to longitudinal velocity variation of model (15), and we made a simple test where we simulated the framework described in Section 3.3 and illustrated in figure 7 considering the "Vehicle" block as the PWA model (15). We choose a simple manoeuvre

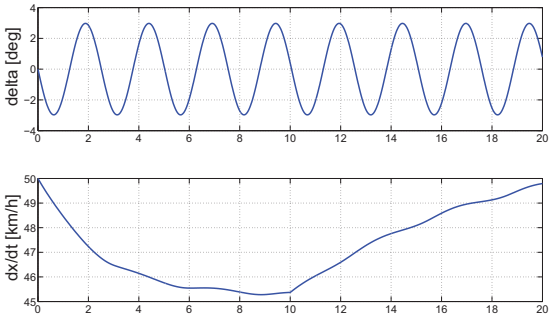

Fig. 8. Input signal for check model simulation. From the top: driver steering wheel angle (SWA) in [deg] and vehicle longitudinal velocity in [km/h].

where the car is driving on icily asphalt condition ($\mu = 0.3$) and the driver imposes a sinusoidal steering profile and changes the position of accelerator pedal such that the vehicle is subject to both deceleration and acceleration as shown in Figure 8. For this case, the tuning parameters are: *(i)* N = 2, *(ii)* sampling time $T_s = 50ms$, *(iii)* the control weight matrix for the states variable ξ is $diag\,[10, 55]$, *(iv)* the control weight matrix R is $diag\,[5 \cdot 10^{-6}, 5 \cdot 10^{-10}]$ and the penalizing steering difference factor ρ is 100. The results, shown in Figure 9, confirm the robustness

of RESC controller, indeed, for all longitudinal variation of v_x the controller is able to compute a control low such that the vehicle is inside the $\mathcal{R}_\infty^1$ set and, in the same time, the state variables track perfectly their respective references, as illustrated in Figure 9 where we reported the tracking behavior and in Figure 10 where are depicted the computed control inputs.

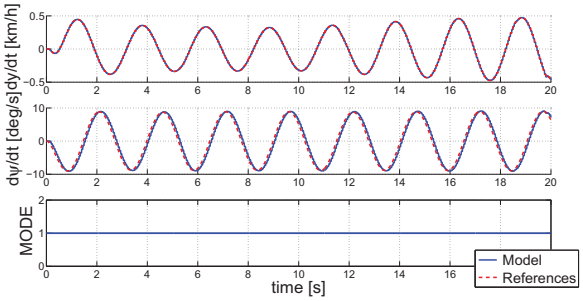

Fig. 9. Results of check control strategy simulation. From the top: a) reference lateral speed (dashed line) versus vehicle lateral speed [km/h]; b) reference yaw rate (dashed line) versus vehicle yaw rate (solid line).

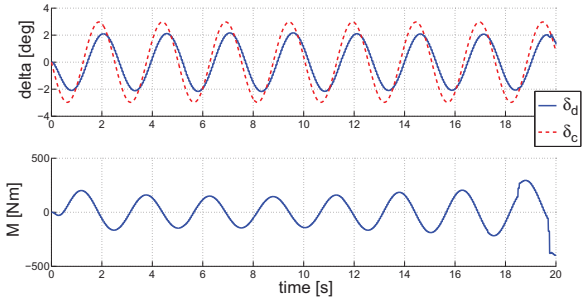

Fig. 10. Results of check control strategy simulation. From the top: a) driver turn wheel angle (dashed line) versus controller turn wheel angle; b) controller braking action.

Furthermore, we tested our control strategy with a high fidelity model of an oversteering sport car from (Falcone et al. [2008]), to verify the possible implementation on real car. In this case we consider a standard test maneuver known as ATI90 in which the driver in turns the steering wheel from $-90deg$ to $90deg$ while not engaging the acceleration pedal.

This maneuver is widely used in lateral vehicle dynamics control tests since the steering profile imposed by driver resembles to the maneuver the driver would use in order to avoid a sudden obstacle. The simulation of the ATI90 maneuver are performed for two different road conditions: dry asphalt (friction coefficient $\mu = 0.9$) and asphalt covered by ice ($\mu = 0.3$). The sampling time for the controller is $T_s = 50[ms]$.

In the "dry scenario", corresponding to the tire–road friction coefficient $\mu = 0.9$, the tuning parameters of the controller (see (31) and (32)) are: state weighting matrix $Q = diag\,[1, 10]$, the control weight matrix $R = diag\left[5 \cdot 10^{-9}, 5 \cdot 10^{-9}\right]$ and factor for penalizing the steering correction $\rho = 50$. Simulation results for the case when the driver controls the vehicle (termed as "open–loop" (OL)) and the case when the controller is active (referred to as "closed–loop" (CL)) are shown in Figure 11.

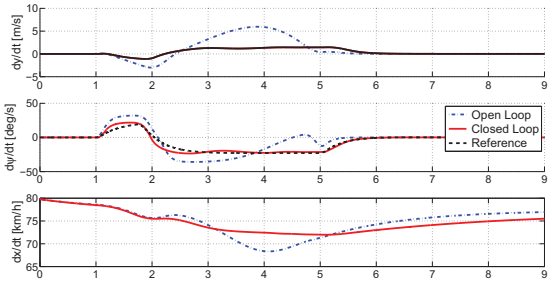

Fig. 11. Chassis behavior. From the top: (a) lateral velocity in open–loop simulation (dot-dashed line), lateral velocity (solid line) and its reference (dashed line) in closed–loop simulation, (b) yaw rate in open–loop simulation (dot-dashed line), yaw rate (solid line) and its reference (dashed line)in CL simulation, (c) longitudinal velocity in open–loop simulation (dot-dashed line) vs longitudinal velocity in closed–loop simulation (solid line)

From Figure 11 we can see a good tracking performance for the closed–loop case and the resulting stability of the lateral vehicle dynamics, compared to the open–loop case where oscillatory behavior in the time interval $[2, 5][s]$ can be seen. In closed–loop case the controller's task is to keep the state trajectory *within* the maximal RCI set $\mathcal{R}_\infty^1$. In doing so, the controller overrides the driver command in order to maintain the desired "stable" lateral motion of the car.

This aspect is evident from Figure 12 depicting the steering and braking profiles for the open– and closed–loop case. When the driver requests a steering angle which would, for the given road conditions and the longitudinal velocity, cause the saturation of the tire–road force on some of the wheels, the controller implements a different steering command and, if necessary, applies the braking momentum in order to preserve the "nominal" car behavior. Thus, we have a difference in steering profile of the driver and the one implemented by the controller, as shown in Figure 12.

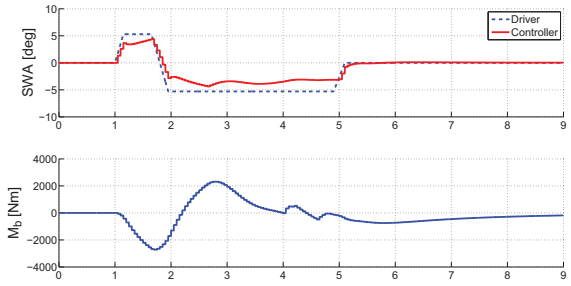

Fig. 12. Control Inputs: a) turn wheel angle of driver (dashed line), turn wheel angle of the controller (solid line), (b) braking moment.

We tested the same maneuver for the icy road conditions. In order to achieve satisfactory performance, a re-tuning of the controller is necessary. The simulations for the icy road are performed with the following controller parameters: $Q = diag\,[25, 145]$, $R = diag\,\left[5 \cdot 10^{-12}, 5 \cdot 10^{-8}\right]$ and $\rho = 20$.

We tested the ability of the controller to compensate for the short–term unmodelled disturbances. In particular, we considered the scenario in which the car passes of the patch of ice with the friction coefficient $\mu = 0.3$ different from the one assumed by the model ($\mu = 0.3$). This is shown in Figure 13. At time $t = 3[s]$ the car passes over the icy surface with lower friction, which cases the transition from the mode 1 to mode 2 for the duration of the disturbance. It can be seen that, after the disturbance is gone, the controller brings the vehicle back to its nominal behavior corresponding to mode 1.

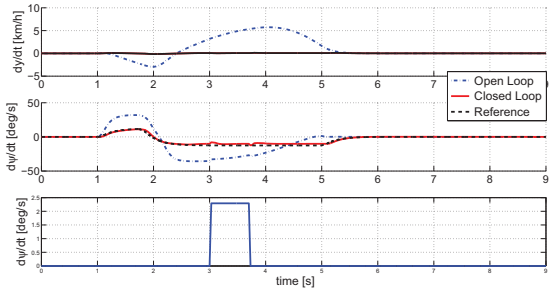

Fig. 13. Chassis behavior. From the top: (a) lateral velocity in OL simulation (dot-dashed line), lateral velocity (solid line) and its reference (dashed line)in CL simulation, (b) yaw rate in OL simulation (dot-dashed line), yaw rate (solid line) and its reference (dashed line)in CL simulation, (c) yaw rate disturbances that simulates a passing over a patch of ice.

In order to restore the nominal car behavior, the controller changes the sign of the braking moment and imposes a slight counter–steering (see Figure 14). Such action is typical for an experienced driver in such situation.

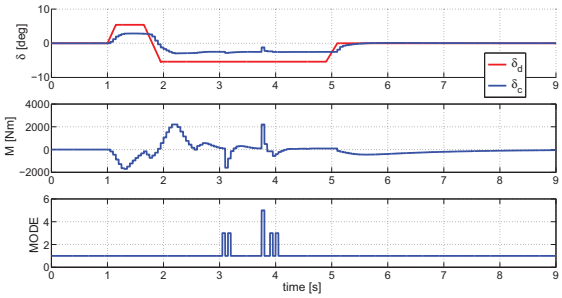

Fig. 14. Control Inputs: a) turn wheel angle of driver (dashed line), turn wheel angle of controller (solid line), (b) braking moment, (c) working mode.

Since the controller is active all the time and has the priority over the driver in controlling the vehicle's behavior, it is required that the steering angle of the controller does not differ much from the desired steering requested by the driver. This makes the controller non–invasive and

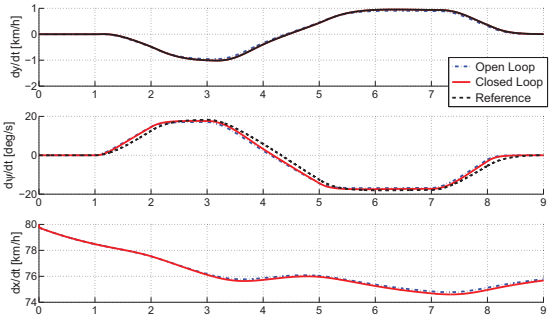

Fig. 15. Chassis behavior. From the top: (a) lateral velocity in OL simulation (dot-dashed line), lateral velocity (solid line) and its reference (dashed line)in CL simulation, (b) yaw rate in OL simulation (dot-dashed line), yaw rate (solid line) and its reference (dashed line)in CL simulation, (c) longitudinal velocity in OL simulation (dot-dashed line) vs longitudinal velocity in CL simulation (solid line), (c) longitudinal velocity

increases the driving comfort. Naturally, the small difference in steering between the driver and the controller can be induced only when the driver's action aligns with the controller's task to keep the vehicle "in mode 1". We tested the behavior of the controller for the dry road scenario and the velocity of 80 [km/h]. The driver performs a smooth, non–aggressive steering profile such that during the open–loop manoeuvre the tire–road forces are not saturated. The behavior of the vehicle for the open– and closed–loop scenario is shown in Figure 15. The car behavior is almost identical for both cases since the controller applies the almost the same steering as the driver and does not deploy the braking (see Figure 16).

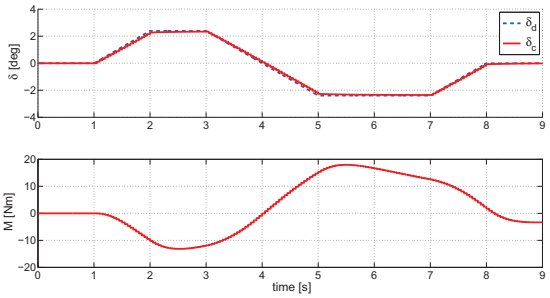

Fig. 16. Control Inputs: a) turn wheel angle of driver (dashed line), turn wheel angle of controller (solid line), (b) braking moment.

5. CONCLUSION

In this paper, a vehicle lateral dynamic control approach has been presented utilizing differential braking and active front steering. The designed controller is able to guarantee constraint satisfaction for all longitudinal speed variations. This paper, together the first work presented by the same authors (Palmieri et al. [2010]) represents a attempt to address hard constraints and uncertainties in the vehicle stability control system in a systematic and rigorous way through a robust constrained control design. A future step

will be to test the control strategy on one prototype and, then, to implement the Algorithm 3 in real time using a quadratic solver and to implement a gain scheduling strategy able to cover range of longitudinal speed variation more the 10 [km/h] and all friction coefficients.

REFERENCES

M. Barić. *Constrained Control: Computations, Performance and Robustness*. PhD thesis, ETH Zürich, 2008.

M. Barić, S.V. Raković, T. Besselmann, and M. Morari. Max-Min Optimal Control of Constrained Discrete-Time Systems. In *Proc. 17th IFAC World Congress*, pages 8803–8808, Seoul, South Korea, July 2008.

D. P. Bertsekas. Infinite-time reachability of state-space regions by using feedback control. *IEEE Trans. Automat. Contr.*, 17:604–613, October 1972.

F. Blanchini and S. Miani. *Set-Theoretic Methods in Control*. Birkhäuser, 2008.

C. Conte. Hybrid control of lateral vehicle dynamics. Master's thesis, Swiss Federal Institute of Technology (ETH Zurich), 2009.

P. Falcone, H. E. Tseng, F. Borrelli, J. Asgari, and D. Hrovat. MPC-based yaw and lateral stabilisation via active front steering and braking. *Vehicle System Dynamics*, 46, Supplement:611–628, 2008.

U. Kienke. *Automotive Control Systems*. Springer–Verlag, 2000.

M. Kvasnica, P. Grieder, M. Baotić, and M. Morari. Multi Parametric Toolbox (MPT). In *Hybrid Systems: Computation and Control*, Lecture Notes in Computer Science. Springer, 2003. URL `http://control.ee.ethz.ch/ mpt`.

J. Löfberg. YALMIP: A toolbox for modeling and optimization in MATLAB. In *Proceedings of the CACSD Conference*, Taipei, Taiwan, 2004. Available from `http://control.ee.ethz.ch/~joloef/yalmip.php`.

NHTSA. Final report: Analysis of the crash experience of vehicles equipped with all wheel antilock braking systems (ABS). 2000.

H. B. Pacejka. *Tire and Vehicle Dynamics*. SAE International and Elsevier, 2005.

G. Palmieri, M. Barić, F. Borrelli, and L. Glielmo. A Robust Lateral Vehicle Dynamics Control. In *10th International Symposium on Advanced Vehicle Control*, 2010.

R. Rajamani. *Vehicle Dynamics and Control*. Springer–Verlag, 2005.

S.V. Raković, M. Barić, and M. Morari. Max-Min Control Problems of Constrained Discrete Time Systems. In *Proc. 47th IEEE Conf. on Decision and Control*, pages 333–338, Cancun, Mexico, December 2008.

A. T. van Zanten, R. Erthadt, and G. Pfaff. VDC, the vehicle dynamics control of Bosch. In *Proc. of International Congress and Exposition*, number 950759 in Proc. of SAE, pages 9–26, Detroit, MI, USA, February 1995.